Battery Power Management in Heavy-duty HEVs based on the Estimated Critical Surface Charge

Tae-Kyung Lee, Youngki Kim, Denise Kramer, and Zoran Filipi*

Abstract:

Real time battery performance in a Hybrid Electric Vehicle (HEV) is significantly affected by the battery allowable power limits. This is particularly true in the case of large vehicles, where rates of energy flows through the system reach up to the marginal values during aggressive acceleration or braking. The underlying phenomenon determining the limits is closely connected to the critical surface charge (CSC) defined by the average positive electrode concentration at the solid particle surface in the cell. This paper characterizes the CSC under high discharging power with respect to the initial battery state of charge (SOC), and subsequently utilizes the insight to propose a novel approach to design supervisory control of a series HEV. The new strategy includes a battery power management logic that prevents battery over-charging and over-discharging under aggressive driving conditions. The CSC estimated by the extended Kalman filter (EKF) is processed with a finite impulse response (FIR) filter to smooth out short-term fluctuations and highlight longer-term trajectories. Then, the filtered CSC sequence is used to determine the battery allowable power limits in real time and feedbacked to the supervisory controller. The proposed strategy is implemented in the heavy-duty HEV simulation framework and its effectiveness is validated under an aggressive real-world military cycle. Undesirable battery operations and potential possibility of the complete Lithium-ion depletion are prevented, thus improving battery health prospects without any penalty on fuel efficiency.

Keywords: Lithium-ion battery; power management; critical surface charge; Lithium-ion concentration; estimation; extended Kalman filter; hybrid electric vehicle.

1 Introduction

Vehicle hybridization is a critical pathway for improving fuel economy of military and commercial trucks. The multiple power sources in the hybridized vehicles provide design and control flexibilities and offer a significant potential for improving fuel efficiency. On-board energy storage(s) and reversible electric machines enable recuperation of braking energy, optimization of engine operation, and engine shut-down on demand. The engine could be downsized, yet this may be limited in the case of large trucks due to the continuous high power requirement for sustaining speed under uphill climbing. The work on hybridization of military vehicles is motivated by the overriding objective to reduce the logistics tail, improve the range of vehicles and reduce cost of large-scale operations. The impetus for the commercial sectors has recently been dramatically enhanced by the impeding new regulation addressing fuel consumption and greenhouse gas emission. The vehicle hybridization is one of the most promising solutions (Carns and Schlesinger, 2008).

Energy conversion options for heavy vehicle hybridization include electric and hydraulic components. Hydraulic hybrid systems have been developed for heavy-duty or

Report Documentation Page		*Form Approved* *OMB No. 0704-0188*

1. REPORT DATE **01 MAR 2011**	2. REPORT TYPE **Journal Article**	3. DATES COVERED **25-07-2010 to 12-01-2011**

4. TITLE AND SUBTITLE **Battery Power Management in Heavy-duty HEVs based on the Estimated Critical Surface Charge**	5a. CONTRACT NUMBER **W56HZV-04-2-0001**
	5b. GRANT NUMBER
	5c. PROGRAM ELEMENT NUMBER
6. AUTHOR(S) **Tae-Kyung Lee; Youngki Kim; Denise Kramer; Zoran Filipi**	5d. PROJECT NUMBER
	5e. TASK NUMBER
	5f. WORK UNIT NUMBER
7. PERFORMING ORGANIZATION NAME(S) AND ADDRESS(ES) **UNIVERSITY OF MICHIGAN,4260 Plymouth Road,Ann Arbor,Mi,48109**	8. PERFORMING ORGANIZATION REPORT NUMBER **; #21551**
9. SPONSORING/MONITORING AGENCY NAME(S) AND ADDRESS(ES) **U.S. Army TARDEC, 6501 East Eleven Mile Rd, Warren, Mi, 48397-5000**	10. SPONSOR/MONITOR'S ACRONYM(S) **TARDEC**
	11. SPONSOR/MONITOR'S REPORT NUMBER(S) **#21551**

12. DISTRIBUTION/AVAILABILITY STATEMENT
Approved for public release; distribution unlimited

13. SUPPLEMENTARY NOTES
Submitted to International Journal of Vehicle Design

14. ABSTRACT

Real time battery performance in a Hybrid Electric Vehicle (HEV) is significantly affected by the battery allowable power limits. This is particularly true in the case of large vehicles, where rates of energy flows through the system reach up to the marginal values during aggressive acceleration or braking. The underlying phenomenon determining the limits is closely connected to the critical surface charge (CSC) defined by the average positive electrode concentration at the solid particle surface in the cell. This paper characterizes the CSC under high discharging power with respect to the initial battery state of charge (SOC), and subsequently utilizes the insight to propose a novel approach to design supervisory control of a series HEV. The new strategy includes a battery power management logic that prevents battery over-charging and overdischarging under aggressive driving conditions. The CSC estimated by the extended Kalman filter (EKF) is processed with a finite impulse response (FIR) filter to smooth out short-term fluctuations and highlight longer-term trajectories. Then, the filtered CSC sequence is used to determine the battery allowable power limits in real time and feedbacked to the supervisory controller. The proposed strategy is implemented in the heavy-duty HEV simulation framework and its effectiveness is validated under an aggressive real-world military cycle. Undesirable battery operations and potential possibility of the complete Lithium-ion depletion are prevented, thus improving battery health prospects without any penalty on fuel efficiency.

15. SUBJECT TERMS

Lithium-ion battery; power management; critical surface charge; Lithium-ion concentration; estimation; extended Kalman filter; hybrid electric vehicle.

16. SECURITY CLASSIFICATION OF:			17. LIMITATION OF ABSTRACT	18. NUMBER OF PAGES	19a. NAME OF RESPONSIBLE PERSON
a. REPORT **unclassified**	b. ABSTRACT **unclassified**	c. THIS PAGE **unclassified**	**Public Release**	**18**	

military vehicle applications because of its high specific power enough to propel the heavy weight (Filipi *et al.*, 2004, 2010; Hui, 2010; Johri and Filipi, 2009; Surampudi *et al.*, 2009; Wu *et al.*, 2004). In contrast, electrification is dominant in the passenger car sector, with many hybrid electric vehicle (HEV) configurations, such as parallel and power-split, already in production. The electric hybrid system started to be spotlighted in heavy-duty vehicles and military vehicle sectors due to the additional benefits, such as the capability for on-board power generation and sustained operation of large electrified accessories, to the fuel economy potential. However, heavy weight and aggressive driving of the heavy-duty or military vehicles lead to high rates of energy flow, and this has been challenges for battery thermal management and life. Safe and reliable operation is often ensured by oversizing battery packs with sufficient safety margin, and that causes the unfortunate cost implications. In summary, battery sizing and control are critical for the vehicle hybridization, and they motivate the development of advanced power management capable of maximizing battery performance, while preventing occurrence of extreme and potentially destructive conditions.

The heavy-duty application requires high specific power and energy, thus, recent advances in Lithium-ion (Li-ion) battery technologies accelerate their use in the electric vehicle (EV) and HEV because of its high-power and high-energy density (Karden *et al.*, 2007). The Li-ion battery has a possible risk of explosion when operated in extreme conditions, such as high temperature and over-charging/discharging. Hence, preventing overcharging and discharging is critical for improving the battery life and stability. Most of the previous studies in simulation-based HEV design optimization and control design rely on simple equivalent circuit battery models because of the simple structure and fast computation (Lin *et al.*, 2003, 2004; Sciarretta *et al.*, 2004, Sharer *et al.*, 2007; Patil *et al.*, 2009, 2010, West *et al.*, 2003). However, the equivalent circuit models cannot predict the Li-ion electrochemical diffusion dynamics, which affects the allowable battery power limits. Therefore, the battery allowable power limits in previous studies are determined only from the battery initial state of charge (SOC) and applied current. The terminal voltage is directly affected by the solid-electrolyte concentration, and high discharge rate results in sudden voltage drop and Li-ion depletion at the boundary of the electrolyte with the solid particles (Di Domenico *et al.*, 2008, 2010). Therefore, estimation of ion surface concentration is critical for assessing limits of battery dynamic operation.

The battery response can be predicted using electrochemical battery models. Electrochemical models of the Li-ion battery were developed by Doyle *et al.* (1993), and further improved in the following studies (Fuller *et al.*, 1994; Gu and Wang, 2000). The full-order electrochemical models can predict the solid concentration profiles across the electrodes and electrolyte, but, their long computational time and the extensive model complexity prevent their application in control design and real-time on-board estimator. Model reductions using the simple electrode-averaged, single-particle model were proposed by Di Domenico *et al.* (2008, 2010), and the averaged model is valid when the concentration distribution along the length of the electrodes and separator can be assumed constant. Regardless of the limitation, the averaged model provides Li-ion concentration profiles in the electrodes and can produce a state-space system with linear dynamics of spherical diffusion in the solid material and a nonlinear voltage output equation (Di Domenico *et al.* 2008, 2010). Thus, the averaged model is useful for the prediction of Li concentration in control design. Accurate battery behavior prediction in the heavy-duty

HEV is a prerequisite for advanced control design to prevent battery degradation and damage.

In this paper, we propose a control strategy to attenuate excessive battery charging and discharging utilizing the critical surface charge (CSC) defined by the average positive electrode concentration at the solid particle surface through the cell. The CSC is estimated by a model-driven extended Kalman filter (EKF). Then, a finite impulse response (FIR) filter is used to process the estimated CSC to smooth out short-term fluctuations and highlight longer-term trajectories. Since the CSC is very sensitive to the applied charging and discharging current, the direct use of the CSC for adjusting the battery allowable power limits is not appropriate. The filtered CSC information is used in the proposed control strategy to adjust the battery allowable power limits.

This paper is organized in the following way: First, a HEV simulation framework to design supervisory control including the electrode-averaged Li-ion battery model is presented in Section 2. Then, the derived electrode-averaged Li-ion battery model is shown in Section 3. Based on the model, battery diffusion dynamics is characterized under high discharging conditions in Section 4. The overall supervisory control structure is presented, and battery power management strategy utilizing the EKF is proposed in Section 5. Then, the effects of the proposed controller on battery responses are reviewed in Section 6 before presenting summary and conclusions.

2 SIMULATION FRAMEWORK FOR CONTROL DESIGN

HEV simulation framework is constructed to obtain realistic responses of each component with the balance of computation time and prediction accuracy. A heavy-duty series HEV equipped with a Li-ion battery is selected as the target vehicle to investigate the effect of the electrochemistry battery dynamics on control design. The heavy-duty series HEV requires high propulsion power due to its large mass. In addition, the propulsion power often comes entirely from an electrical sub-system, thus leading to frequent peak loads. Table 1 shows the specification of the target vehicle. The component sizes were initially determined to satisfy the performance targets: maximum speed, gradeability, and acceleration. Rolling resistance, drag, and grade terms are taken into account in the vehicle power demand.

$$m_e \dot{v}_{veh} = F_{prop} - F_{RR} - F_{WR} - F_{GR}, \tag{1}$$

where F_{net} is the net force applied to the vehicle, F_{prop} is the propulsion force from the powertrain, F_{RR} is the rolling resistance force, F_{WR} is the wind resistance force, F_{GR} is the grade resistance force and all other external forces applied to the vehicle, m_e is the equivalent vehicle mass, v_{veh} is the vehicle velocity, and a_{veh} is the vehicle acceleration.
Figure 1 shows the overall vehicle simulation framework. The vehicle simulation is forward looking, as the driver determines control commands to follow desired velocity profiles. The supervisory controller assigns propulsion and braking power to the engine and the motor respectively. Then, the electric power demand to the battery is determined as

$$P_{batt} = -P_{egn} + P_{mot} + P_{accs}, \tag{2}$$

Table 1. Heavy-duty Series-HEV Specification: Hybridized M-ATV

	Specification
Vehicle	Hybridized M-ATV
Weight	13,400 kg
Payload	1,814 kg (4000 lbs)
Frontal area	5.72 m^2 (Width/Height: 2.49/2.70 m)
Engine	I6 Turbo-diesel engine: 275 kW
Generator	Permanent Magnet: 275 kW
Battery	Li-ion 5.0 ~ 13.0 kWh
Motors	Permanent Magnet: 380kW

Figure 1 Simulation frame work of the series hybrid electric vehicle in SIMULINK with a forward-looking approach.
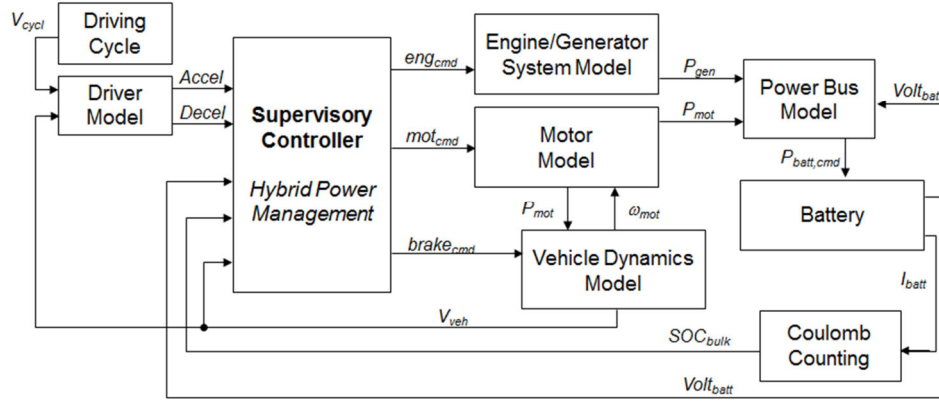
where P_{batt} is the battery output power, P_{mot} is the motor output power, P_{eng} is the engine output power, and P_{accs} is electric accessory power. The required P_{batt} determines the current input to the battery, $I_{inp.batt}$, using the battery terminal voltage, V_{batt}, and the terminal voltage is calculated from 98th order averaged electrochemistry battery model. We note that the only input to the battery cell model is "current" and the only output to the battery cell is "terminal voltage", just like in a real vehicle.

2.1 Engine

Map-based engine model is used to reduce the computation time, and it is sufficient for the HEV fuel economy prediction. The engine is assumed to be fully warmed up and its operating point is controlled to follow the optimal *bsfc* line for a given power demand through regulating the generator torque in real time. Thus, the desired engine speed ω_e and engine torque T_e can be determined for any power requirement. The mass of fuel injected per cycle needs to correspond precisely to the instantaneous operating condition. Therefore, inverting the torque function $T_e = f_{eng,T}\left(\omega_e, \dot{m}_f\right)$ provides the fuel consumption rate as a function of engine speed and engine torque.

$$\dot{m}_f = f_{eng,T}^{-1}\left(\omega_e, T_e\right) = f_{eng,fuel}\left(\omega_e, T_e\right) \tag{3}$$

Total fuel consumption is calculated by integrating fuel consumption rate over the time period. Engine speed is calculated based on rotor dynamics by combining generator inertia with engine inertia.

2.2 Electric Motor/Generator

The outputs of the electric motor/generator are determined depending on operating conditions. The efficiency of the electric machine is assumed to be a function of the operating speed ω_{elec} and torque T_{elec} (or power P_{elec}). The efficiency is generally measured through experiments. In the simulation work, quasi-steady state nonlinear efficiency maps are used to compute the output power expressed as:

$$P_{\text{mech}} = P_{\text{elec}} \cdot \eta_{\text{em}} \quad \text{(discharging)} \tag{4 a}$$

$$P_{\text{elec}} = P_{\text{mech}} / \eta_{\text{em}} \quad \text{(charging)} \tag{4 b}$$

where $\eta_{em} = \eta_{em}\left(\omega_{elec}, T_{elec}\right)$, or $\eta_{em} = \eta_{em}\left(\omega_{elec}, P_{elec}\right)$ is the electric motor efficiency. Each maximum and continuous torque operation limit is assumed to a function of speed. Electrical dynamics are supposed to be sufficiently faster than vehicle dynamics.

3 Electrode-Averaged Battery Model

Li-ion battery cells are modeled by describing the key dynamics of charging and discharging in the electrodes. The electrode-averaged electrochemistry model is

Figure 2 Illustration of Li-ion battery models: (a) macroscopic (x-direction) cell model with coupled microscopic solid diffusion model (r-direction), (b) electro-averaged cell model with coupled microscopic solid diffusion model (r-direction)

(a)

(b)
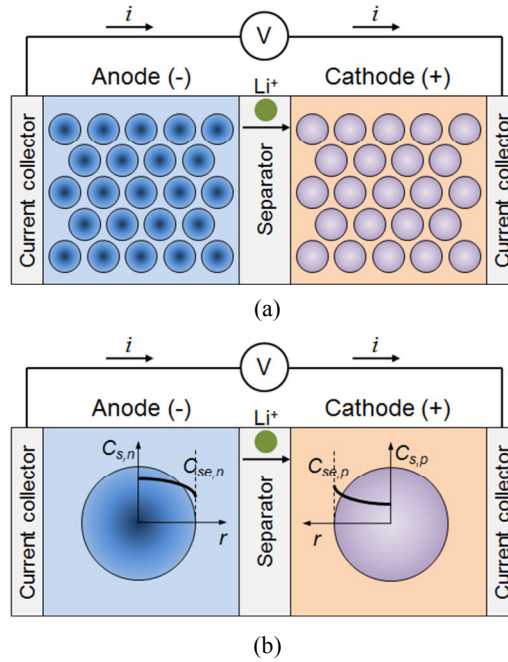
developed, where Li-ion concentration change between the solid particles in the electrode is neglected, and the concentration in the electrolyte concentration is assumed to be constant. The lack of spatial resolution within the electrode might be a factor under high charging and discharging conditions, but the diffusion dynamics in the solid particle capture the critical aspects of battery behavior with sufficient accuracy for controller development.

Figure 2 (a) shows the general structure of a Li-ion battery. It consists of three parts: two porous electrodes, cathode and anode, and a separator between those two electrodes. The potential energy difference in each electrodes generate voltage, and Li-ions have the lowest potential energy when interstitial sites within the solid crystalline structure of the cathode. During the charging process, Li-ions are forced to move from the cathode to the anode. The Li-ions diffuse to the surface within the cathode's solid structure, then, traveling through the electrolyte across the separator, and entering into the anode. During the discharging process, the Li-ions diffuse into the anode's interstitial sites.

The diffusion process can be expressed by a set of ordinary differential equations (ODE) by using the finite difference method for the spatial variable r in order to be used as the battery control oriented model (Di Domenico *et al.* (2008, 2010)). The sphere radius is divided by M_r-1 intervals. The system states are distributed Li-ion concentration in the solid, $c_s = (c_{s,1}, c_{s,2}, \ldots, c_{s,Mr-1})^{\mathrm{T}}$. The resulting state-space equation is expressed as

$$\dot{c}_s = A c_s + B u , \tag{5}$$

where A is a constant tri-diagonal matrix determined from

$$\dot{c}_{s,k} = \frac{2 D_s}{\Delta_r^2} \left[\left(\frac{k-1}{k} \right) c_{s,k-1} - 2 c_{s,k} + \left(\frac{k+1}{k} \right) c_{s,k+1} \right] , \tag{6}$$

for $k=1, \ldots M_r-1$, and $\Delta_r = R_s /(M_r -1)$, with boundary conditions:

$c_{s,0} = c_{s,1}$ and $c_{s,e} = c_{s,Mr} = c_{s,Mr-1} - \Delta_r \dfrac{\overline{j}^{Li}}{F a_s D_s}$ at the solid particle surface, $\overline{j}^{Li} = I / \delta A$ is

the electrode-average current flux.

The battery voltage, using the average values at the anode and the cathode, can be written as

$$V = \left(U_p \left(\theta_p \right) - U_n \left(\theta_n \right) \right) - \frac{K_r}{A} I + \eta(c_{se,p}, c_{se,n}, I) , \tag{7}$$

where $K_r = \dfrac{I}{2 k^{\mathit{eff}}} (\delta_n + 2 \delta_{sep} + \delta_p) + R_f$ is a term accounting for both internal and collector film resistances, k^{eff} is the effective electrolyte phase conductivity, δ is the electrode thickness with subscripts p and n referring to the cathode and the anode, and η is the overpotential

$$\eta(c_{se,p}, c_{se,n}, I) = \frac{RT}{\alpha_a F} \ln \frac{\xi_p + \sqrt{\xi_p^2 + 1}}{\xi_n + \sqrt{\xi_n^2 + 1}} , \tag{8}$$

where $\xi_p = \overline{j}_p^{Li} / 2 a_s j_{o,p}$, $\xi_n = \overline{j}_n^{Li} / 2 a_s j_{o,n}$.

4 Battery Diffusion Dynamics Characterization

The Li-ion concentration prediction by the electrode-averaged battery model enables more sophisticated battery management to prevent excessive battery charging and discharging. The available power limits are varying depending on the applied current, the initial battery SOC, and the current Li-ion concentration profile. The variance is related to the Li-ion concentration at the solid particle surface. When high current is drawn from a battery, Li-ion surface concentration drops rapidly until the terminal voltage drops to the lower limit, although the bulk SOC estimated by coulomb counting remains within the battery operating range and indicates that the battery can provide current. Thus, characterization of realistic battery responses under charging and discharging at different initial battery SOC is a prerequisite to determine the available power limits under various operating conditions.

Figure 3 Empirical open-circuit potentials at anode and cathode.
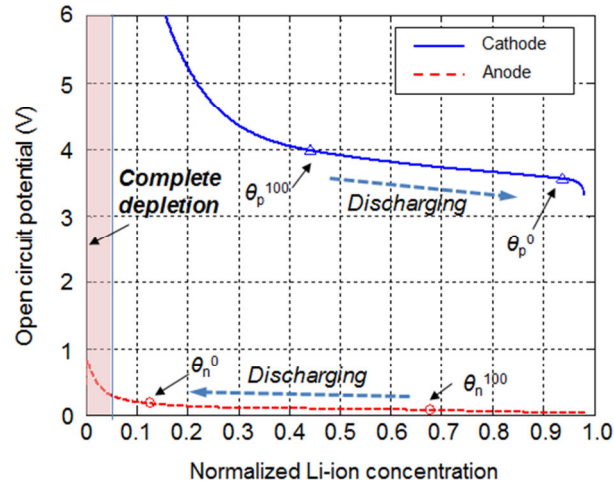
The battery terminal voltage is generally used to determine the battery operating range, thus, we first investigate the battery operating voltage ranges. The battery terminal voltage is calculated from eqn. (7) and a function of open circuit potential. Figure 3 shows the trends of open circuit potential with the negative electrode that consists of Li_xC_6 while the positive electrode consists of $Li_yMn_2O_4$, Li_yCoO_2, Li_yNiO_2, or some combination of metal oxides (Smith and Wang, 2006a, 2006b). The normalized Li-ion concentration ranges are determined from the empirical correlations. Superscripts 0 and 100 represent 0% and 100% SOC, and subscript p and n represent the cathode (positive) and the anode (negative) respectively. Under the charging condition, the terminal voltage can be used as a good criterion to prevent the Li-ion depletion at cathode under charging. Sudden Li-ion concentration variation around the Li-ion concentration of θ_n^{100} and θ_p^{100} will not cause sudden terminal voltage change. The magnitude of resulting charging current is not sensitive to the demanding charging power. Thus, the battery is not suddenly overcharged with excessive current. In contrast, negative open circuit potential changes rapidly under discharging conditions when the normalized concentration decreases below 0.05 as shown in Fig. 3. Small perturbation of the Li-ion concentration

Figure 4 Comparison of terminal voltage drops simulated from the full-order Li-ion battery model and the electrode-averaged Li-ion battery model under high discharge condition: (a) at 0.5 of initial SOC; (b) at 1.0 of initial SOC.
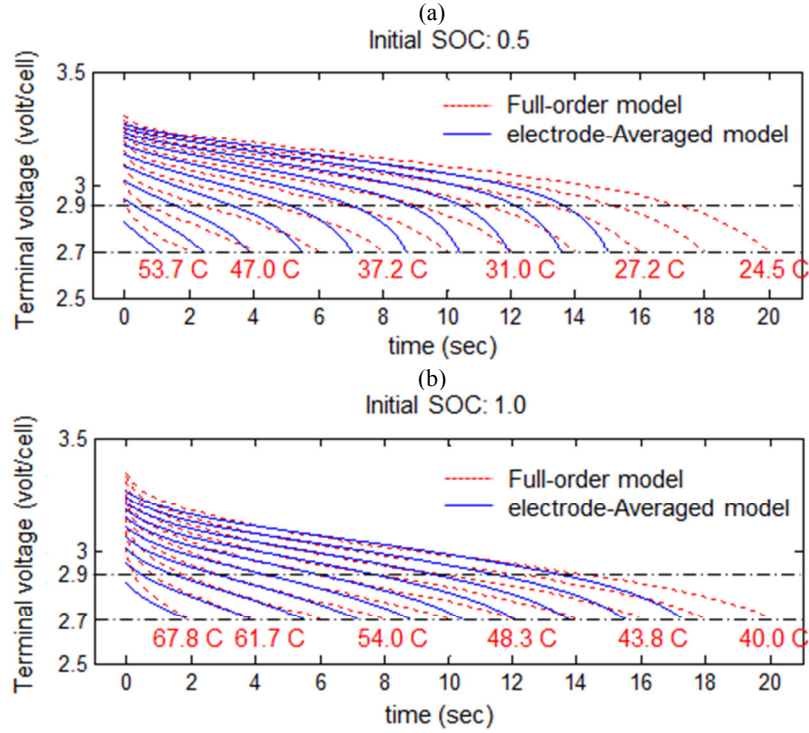
variation below the 0.05 of the normalized concentration will cause sudden terminal voltage drops and subsequent over discharging even at constant discharging power demand. The observation implies that limiting the allowable lowest concentration at the anode is critical to prevent sudden drops of terminal voltage and complete Li-ion depletion. Thus, using the Li-ion concentration information is essential for ensuring safe battery operation at discharging conditions.

In this paper, the battery behavior is predicted from electrode-averaged Li-ion battery simulation under high discharging conditions with the assumption that the initial Li-ion concentration profiles are set to be constant along the anode solid particle radius. Predictions enable delicate management of battery operation to prevent over charging and over discharging. The accuracy of the electrode-averaged Li-ion battery model is validated through comparisons with the full-order electrochemical battery model develop by Smith and Wang (2005). The predictions of the discharge duration within allowed battery operating range obtained with the full and electrode-averaged model are shown in Figure 4. The full-order model includes Li-ion diffusion dynamics in the electrolyte and electrode solids are distributed along the electrode direction, thus, providing the capability of capturing detailed physics in the Li-ion battery with the expense of computational efforts. Under mild discharging condition, the Li-ion concentration change along the electrolyte is relatively small compared to the high discharging conditions (Di Domenico 2008, 2010), and the electrode-averaged model demonstrates sufficient

Figure 5 Normalized Li-ion surface concentration predicted by the electrode-averaged electrochemical Li-ion battery model with respect to initial bulk SOC and applied discharging power.
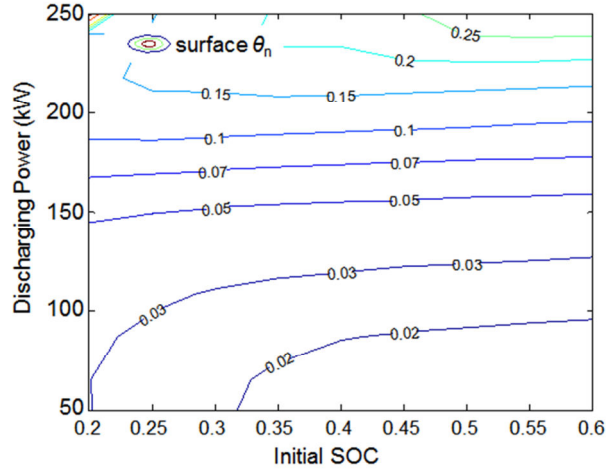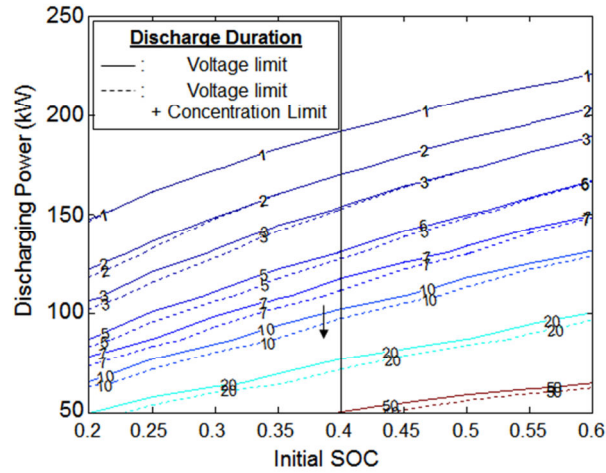

Figure 6 Predicted discharging duration under various discharging power at two battery operation limitation strategies; limiting surface concentration(solid), and terminal voltage(dashed).

accuracy. In contrast, under the high discharging condition, electrode-averaged battery model predicts faster terminal voltage drops below 2.9V than the full-order model (see Fig. 4). Initial voltage drops (just after 0 second) from the electrode-averaged model are also lower. The faster voltage drops make the prediction of battery responses conservative in a view of control design since battery operation limits are constrained by pre-determined operating voltage limits. Therefore, model can be used with confidence in ultimately achieving a robust in control design.

Figure 5 shows the normalized Li-ion surface concentration at the anode when the terminal voltage dropped to the low limit (2.7 volts). When the applied discharging power is increasing, the surface concentration also tends to increase at the lower voltage limit. The different Li-ion surface concentration can be explained as follows: Higher

power demand requires higher current, and the voltage drop from the internal resistance becomes higher. Hence, the terminal voltage reaches the lower limit although the Li-ion concentration remains relatively high with the higher discharging current. In contrast, in the low discharging power condition, the Li-ion concentration hits the low value (θ_n= 0.02) while the terminal voltage still satisfies the lower limit of the battery operating voltage. The value 0.02 is close to the complete depletion (θ_n = 0.00). It is not clear how large the safety margin should be, nevertheless, Li-ion surface concentration needs to be utilized for the battery management under dynamic operating conditions.

Available discharging durations are shown in Fig. 6 at two different battery operating range limitation criteria: (1) the terminal voltage low limit (2.7 volts), and (2) the terminal voltage low limit (2.7 volt) and the Li-ion concentration limit (θ_n= 0.05). The tentative criterion is set to θ_n= 0.05 regarding the observation that θ_n increases rapidly below the criteria as shown in Fig. 3. Under the high discharging power above 150 kW, the terminal voltage limit acts as an active battery operation constraint. Thus, the discharging duration is not shortened by the Li-ion concentration limit. In contrast, the concentration limit becomes active with relatively small discharging power below 150 kW as shown in Fig. 5. Hence, the discharging duration needs to be reduced to prevent Li-ion depletion below the tentative criterion of θ_n= 0.05. The additional criterion makes the battery operation more conservative and beneficial to Li-ion battery applications under highly aggressive operations. A novel battery management strategy utilizing the Li-ion concentration information is introduced in the next section.

5 Supervisory Control Design

The supervisory controller is designed by augmenting the thermostatic SOC control strategy with additional logic for limiting potentially harmful charging/discharging power. The controller consists of four driving modes, and it distributes the power from driving cycles to the engine and the battery depending on either SOC (energy), or demanded rates of charging/discharging (power). The modes and rules are summarized as follows:

(1) Electric mode

if $0 < P_{dem} < P_{batt.max}$, and $\text{SOC}_{batt} > \text{SOC}_{ub}$,

$\quad\quad P_{mot} = P_{dem}, \ P_{eng} = 0, \ P_{batt} = P_{mot} + P_{accs}$.

where $P_{batt.max}$ is the maximum allowable battery power. $P_{batt,max}$ has been expressed as a function of the battery SOC (SOC_{batt}) and the battery current in most of previous studies for simplicity. In this paper, we introduce a battery management strategy that adjusts $P_{batt.max}$ utilizing the filtered CSC, and the detail is shown in section 5.2. SOC_{ub} is the upper bound of the SOC dead-band in the thermostatic control (-see Fig. 7). SOC_{lb} is the lower bound of the SOC dead-band in the thermostatic control. This mode will be active when power demand is within the battery discharging capacity and the SOC_{batt} is higher than SOC upper bound (SOC_{ub}).The engine does not provide power to the generator, and the battery provides the entire propulsion power.

(2) Thermostatic control mode

if $0 < P_{dem} < P_{batt.max}$, and $\text{SOC}_{batt} < \text{SOC}_{ub}$,

$\quad\quad P_{mot} = P_{dem}, \ P_{eng} = f(\text{SOC}_{batt})$ in Fig. 7,

$$P_{batt} = -P_{eng} + P_{mot} + P_{accs}.$$

When the driving power demand is within the allowable battery power range, the thermostatic SOC control strategy is applied to manage the battery SOC. The predetermined engine power is used for charging battery to obtain the target threshold SOC (SOC_{ub}). The engine power is limited to the sum of required power for the propulsion and battery charging capacity.

(3) Power mode
if $P_{dem} > P_{batt.max}$
$$P_{mot} = P_{dem}, \quad P_{eng} = P_{mot} + P_{accs} - P_{batt.max},$$
$$P_{batt} = P_{batt.max}.$$

Additional power exceeding the maximum battery power is produced by the engine, and in that case the engine operation is based on the load-following control strategy. The battery power limits are traditionally implemented as functions of the battery SOC. However, discussion in the previous section suggests strong dependency of electrode particle surface concentration on dynamic charging and discharging conditions. Hence, the key new element in our approach is to take that into consideration and feedback the estimated dynamic power limit to the HEV controller. This is further elaborated in the next two sub-sections.

(4) Braking mode
if $P_{batt.min} < P_{dem} < 0$
$$P_{mot} = P_{dem}, \quad P_{eng} = 0, \quad P_{batt} = P_{mot} + P_{accs}.$$
else if $P_{dem} < P_{batt.min}$
$$P_{mot} = P_{batt.min}, \quad P_{eng} = 0,$$
$$P_{mech.brk} = P_{dem} - P_{mot},$$
$$P_{batt} = P_{mot} + P_{accs}.$$

where $P_{batt.min}$ is the minimum allowable battery power. When negative power demand is requested by the driver, regenerative braking mode is activated. When power demand exceeds the regenerative charging capacity which is either battery charging capacity or motor capacity, the mechanical brakes are used to absorb the remaining negative power.
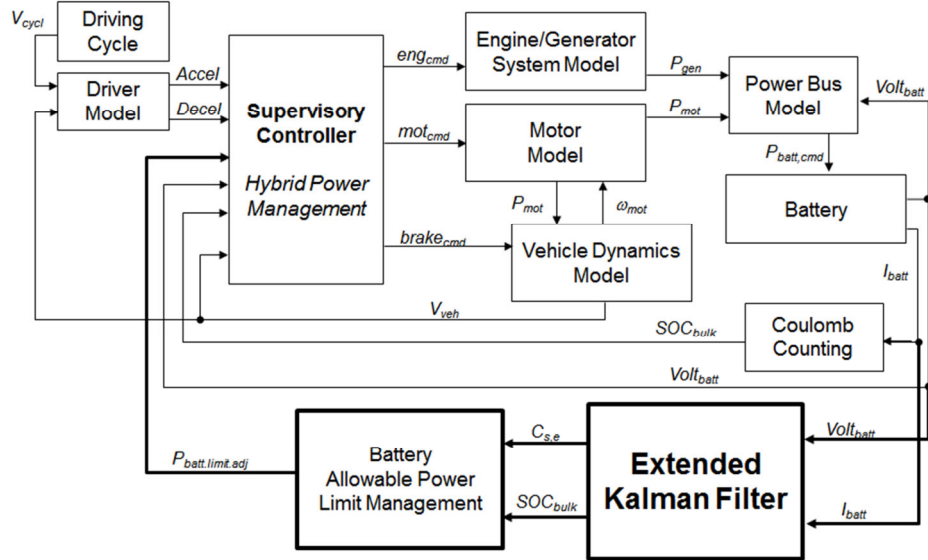
Figure 7 Illustration of the thermostatic SOC power management control
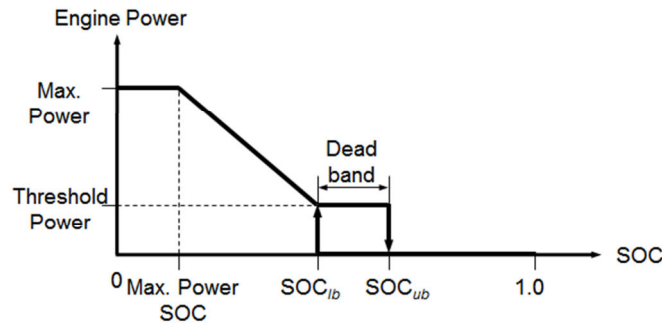
Figure 8 Schematic diagram of the controller structure for battery power limits management using electrochemistry battery model-driven extended Kalman filter.

The thermostatic SOC control strategy has been used in series hybrid hydraulic vehicle (HHV) and HEV control design in several previous studies (Patil et al., 2010; Filipi and Kim, 2009). It is very effective in managing SOC, and providing efficiency gains when combined with optimal engine operating scheme that keeps operating points on the best *bsfc* (braking specific fuel consumption) line (Filipi and Kim, 2009). The basics of the thermostatic SOC control are illustrated in Fig. 7. Whenever the battery SOC hits the lower limit denoted on SOC_{lb} in Fig. 7, the engine begins charging the battery with the threshold power until the battery SOC reaches to the SOC_{ub}. When the battery SOC is lower than the SOC_{lb}, the engine power demand is determined depending on the current SOC as shown in Fig. 7, and threshold power. The engine power is delivered with a combination of torque-speed that keeps the engine operated on the best *bsfc* line for the minimum fuel consumption.

Battery allowable power limit management strategy is augmented to the supervisory controller in order to prevent excessive battery operations. The augmented controller accounts for the battery diffusion dynamics in determining the battery allowable power limits ($P_{batt,max}$ and $P_{batt,min}$). When driving power demand (P_{dem}) exceeds the battery power limits, the operation is shifted to "power mode", thus, preventing battery over-charging and over-discharging. It will be shown that the instantaneous power limits may depart significantly from the nominal for very dynamic events.

High current discharging causes a sudden Li-ion concentration change at the surface of the solid material, thus, resulting in sudden voltage drop. Terminal voltage of the battery is sensitive to both the bulk SOC and Li-ion solid surface concentration. In contrast, high current charging causes a sudden voltage rise. The key to the successful implementation is prediction of allowable battery power limits using the estimated CSC. The estimation is realized by the electrochemical model-driven extended Kalman filter (EKF). The schematic diagram of the controller structure is shown in Fig. 8. The allowable battery

power limits are adjusted by the "power mode" control and fed into the supervisory controller. Then, the supervisory controller distributes the demanding power to the engine and battery using the rules.

5.1. Extended Kalman Filter

The electrode-averaged model based EKF design proposed by Di Domenico et al. (2010) is used to estimate the CSC. The model is expressed as

$$\dot{\hat{x}} = A_p\hat{x} + B_p u + K_e(y - \hat{y}) ,$$
$$\hat{y} = V(\hat{x}, u)$$

(9)

where $\hat{x}$ and $\hat{y}$ are the estimate state x and output y, and the state $x = (\overline{c}_{s,p1}, \overline{c}_{s,p2}, \ldots, \overline{c}_{s,p(M_r-1)})^T$, and output $y = V(x, u)$. The matrices A_p and B_p are obtained from eqn. (15). The nonlinear output is linearized by $C = \partial V/\partial x$, which is a row matrix with zeros in its first M_r-2 elements. The last non-zero term is numerically computed from $\partial V / \partial \overline{c}_{s,p(M_r-1)}$ in the EKF.

The Kalman gain is obtained by

$$K_e = PCR^{-1} ,$$

(10)

where P is the solution of the Ricatti equation

$$\dot{P} = A_p P + PA_p^T - PCR^{-1}C^T P + Q ,$$
$$P(0) = P_0$$

(11)

and Q and R are positive definite matrices to obtain small battery voltage prediction errors. the designed filter is capable of estimating the Li-ion concentration with sufficient accuracy over the entire battery operating range. The performance of the EKF was validated with experimental data by Di Domenico et al. (2010) and the EKF is used to estimate the CSC in this study.

5.2 Battery Power Management Strategy based on dynamic power limits

We propose a battery power management strategy that adjusts the amount of the battery power limits utilizing the information of the filtered CSC information. The FIR filter is used to remove the high frequency fluctuations and to capture long-term trends. In this paper, the same constant filter coefficients are used in the FIR filter. Thus, the final structure is same as a moving average filter. The order of the filter is set to the smallest number that makes the filtered signal show little high frequency fluctuation component while tracking the averaged trajectory.

The control command for the modification of the allowable battery power limits is computed through the feedback of the following cost function,
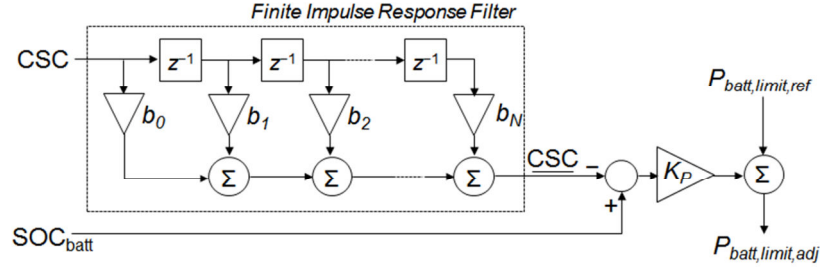
$$J = \underline{\text{CSC}} - \text{SOC}_{batt}$$

(12)

where $\underline{\text{CSC}}$ is the filtered CSC obtained from the FIR filter,

Figure 9 Schematic diagram of the battery power management strategy using the filtered CSC response.

$$\underline{\text{CSC}} = \sum_{k=0}^{N} b_k \text{CSC}(t - k\Delta t) \qquad (13)$$

where Δt is the sampling time, N is the filter order, and b_k is the filter coefficient. The adjustment amount of the battery allowable power $\Delta P_{batt,limit}$ is determined by

$$\Delta P_{batt,limit} = P_{batt,limit,adj} - P_{batt,limit,ref} = K_P J \qquad (14)$$

where $P_{batt,limit,adj}$ is the adjusted battery power limit, $P_{batt,limit,ref}$ is the battery power limit without the consideration of Li-ion diffusion dynamics, and K_p is the proportional control gain, which is determined to constrain the terminal voltage within the battery operation limits (2.7~3.9 volt). $P_{batt,limit,ref}$ is a function of the battery SOC and the battery current. Figure 9 shows the structure of the proposed battery power management strategy. In this study, b_k is set to $1/N$.

Figure 10 shows the comparison of the CSC, the bulk SOC, and the filtered CSC with 9 kWh capacity Li-ion battery under the aggressive urban assault cycles. The CSC shows huge fluctuations below 0.2 and over 0.65 although the bulk SOC changes around 0.4 over the entire cycle. The CSC also has high frequency fluctuation components sensitive to the battery power demand. The high frequency components are smoothened in the filtered CSC response. The FIR filter is designed to partially consider the Li-ion diffusion toward to center of the solid particle, which affects the battery allowable power limits, in addition to the CSC change. Clearly, dynamic predictions of battery power limits are needed as feedback to protect the battery from stepping over critical CSC values.

Figure 10 Comparison of the trajectories of bulk SOC, CSC, and filtered CSC with 9 kWh capacity Li-ion battery without battery allowable power management under urban assault cycle driving.
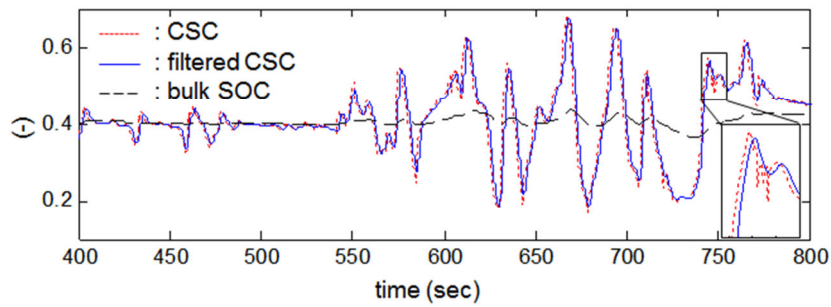
Figure 11 Urban assault driving cycle velocity profile.
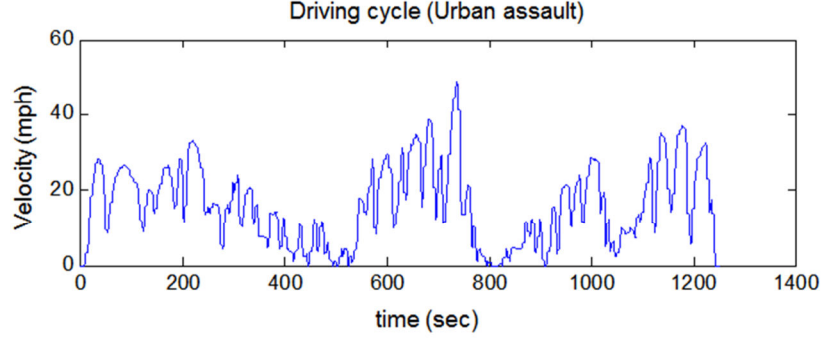

6 Simulation Results

The proposed battery power management strategy enables robust battery operation under aggressive vehicle driving. Parameters of the thermostatic controller, such as the SOC_{lb} and the dead-band width, are heuristically determined to obtain good fuel economy not too sensitive to driving cycle patterns. Simulations with two different supervisory controls are executed with 5 kWh Li-ion battery under the urban assault driving cycle. The urban assault driving cycle is shown in Fig. 11. The cycle consists of frequent acceleration and deceleration, hence, resulting in aggressive driving. The instantaneous power demand is quite high, and the high power demand suddenly drops the CSC and eventually causes complete Li-ion depletion. The real-time adjustment of the allowable battery power limits improves the battery robust operation and prevents the extreme battery operation.

To illustrate the performance of the proposed control design, the baseline is established with a controller that does not incorporate active battery power management. In that case, simulation predicts instances of battery being completely discharged, e.g. around ~210 seconds.. However, Fig. 12(b) shows allowable power limits adjusted in real time to keep the battery terminal voltage within the operation voltage range limits. During sudden acceleration and deceleration, the magnitudes of power limits are significantly contracted. The allowable power limits under discharging is reduced up to 75%, and the limits under charging is adjusted close to zero at extreme as shown in Fig. 12 (a). If these limits are respected, complete Li-ion depletion will be prevented. Otherwise, the battery is overcharged, thus, resulting higher current drops the battery voltage suddenly and causes complete Li-ion depletion at the anode.

The battery current inputs and voltage outputs are compared in Fig. 12 (b) and Fig. 12 (c). Under the mild driving, battery responses are exactly same with or without the battery power management. Under aggressive driving, the proposed controller limits the battery power demand to prevent excessive rates of discharging or charging. Thus, the voltage range is kept within the allowable range. Without the battery power limit adjustment, the voltage fluctuation shown with a dashed line in Fig. 12(c) crosses occasionally the boundaries allowed operation range (2.7V~3.9V). As an example, the voltage exceeds the upper bound (around 47 seconds) due to excessive regeneration braking. Under the severe acceleration, the uncontrolled battery current inputs lead to severe voltage drop (around 210 seconds), and at that point the battery cannot handle the

Figure 12 Battery responses under transient by the proposed battery management strategy using the estimated Li-ion concentration by the EKF with 5 kWh Li-ion battery: (a) battery power limits; (b) battery current inputs; (c) battery voltage outputs

(a)

(b)

(c)
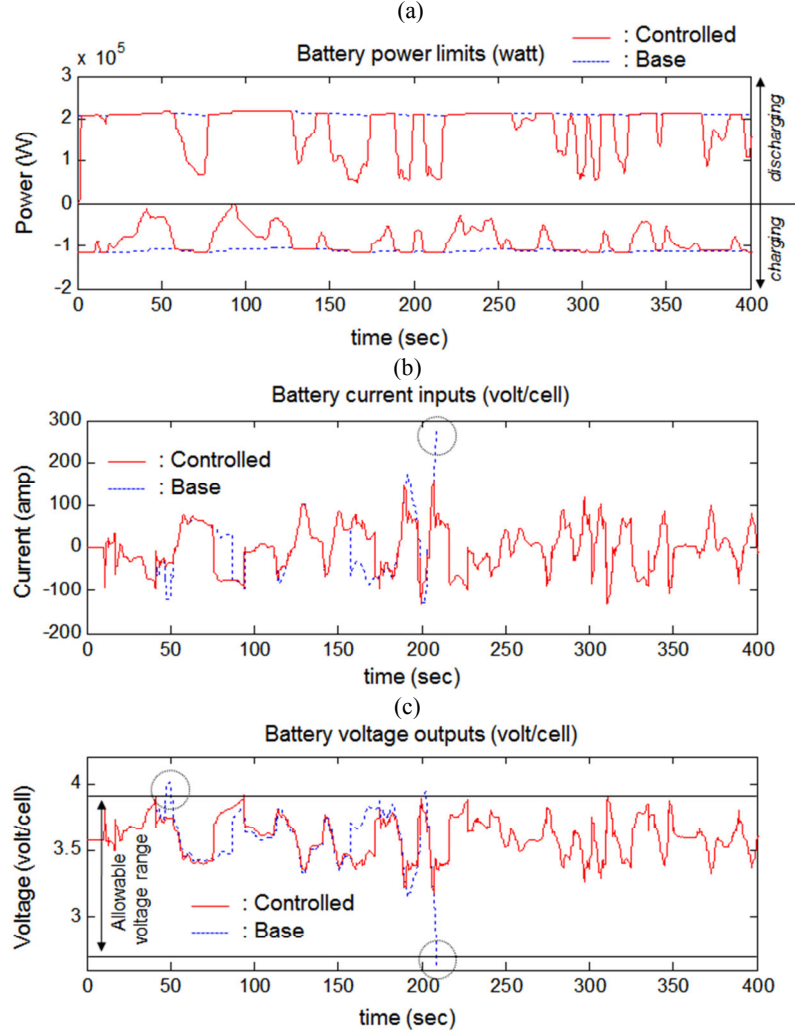
power demand. These peaks are avoided with the battery power management logic; thus, the proposed strategy enables robust and secure battery operation under fast transient and aggressive driving conditions.

7 Conclusions

A model-based Li-ion battery control strategy using estimated critical surface charge (CSC) is proposed to prevent excessive battery charging and discharging in a series hybrid electric vehicle. The series-HEV simulation framework includes an electrode-averaged Li-ion battery model with finely discretized electrode solids to capture the realistic battery voltage drops with respect to applied current. The base supervisory controller has four different operating modes, and the modes are changed based on

driving conditions. The thermostatic SOC control strategy is used to distribute the power between the engine and the battery. The controller is augmented by the proposed battery management strategy that modifies the allowable battery power limits by using the estimated Li-ion concentration at the electrode solid surface (CSC) to represent battery electrochemical dynamics. The final controller adjusts the allowable power limits in real time during highly dynamic charging or discharging events, thus ensuring safe and robust battery operation during aggressive driving conditions. Instances of over-charging or over-discharging are successfully prevented. This enables minimizing the battery size and cost without any significant loss of performance or reliability.

The following provide a summary of the modeling and controller development. The CSC used in the control design is estimated by the electrochemical model-driven extended Kalman filter (EKF). The estimated CSC is then manipulated using the FIR filter to remove fast transient fluctuations and to track the long-term trends. The allowable battery power limits is modified through the feedback of the filtered CSC from the bulk Li-ion concentration. The feedback gain is determined to constrain the resulting terminal voltage within the battery operation limits (2.7~3.9 volt).

Acknowledgement

References

Carns, M. P. C., and Schlesinger, J. (2008) 'Final Report of the Defense Science Board Task Force on DoD Energy Strategy', memorandum for the Chairman, Defense Science Board, Washington, DC, Jan. 14, pp. 3-5.

Di Domenico, D., Fiengo, G., and Stefanopoulou, A. (2008) 'Lithium-ion battery state of charge estimation with a kalman filter based on a electrochemical model', *Proc. 2008 IEEE Conf. Control Applications*, vol. 1, pp.702-707.

Di Domenico, D., Stefanopoulou, A., and Fiengo, G. (2010) 'Reduced order lithium-ion battery electrochemical model and extended Kalman filter state of charge estimation', *ASME J. Dynamic Systems, Measurement and Control - Special Issue on Physical System Modeling*.

Doyle, M., Fuller, T., and Newman, J. (1993) 'Modeling of Galvanostatic Charge and Discharge of the Lithium/polymer/insertion Cell', *J. Electrochemical Society*, vol. 140, pp. 1526-1533.

Filipi, Z., and Kim, Y. J. (2009) 'Hydraulic Hybrid Propulsion for Heavy Vehicles: Combining the Simulation and Engine-in-the- Loop Techniques to Maximize the Fuel Economy and Emission Benefits', *Oil & Gas Science and Technology*, vol. 65. no. 1, pp. 155-178.

Filipi, Z., Louca, L., Daran, B., Lin, C.-C., Yildir, U., Wu, B., Kokkolaras, M., Assanis, D., Peng, H., Papalambros, P., and Stein, J. (2004) 'Combined optimization of design and power management of the hydraulic hybrid propulsion system for the 6×6 medium truck', *Int. J. Heavy Vehicle Systems*, vol. 11, no. 3, pp. 371–401.

Fuller, T. F., Doyle, M., and Newman, J. (1994) 'Simulation and optimization of the dual lithium ion insertion cell', *J. Electrochemical Society*, vol. 141, no. 1, pp. 1-10.

Gu, W. B., and Wang, C. Y. (2000) 'Thermal and electrochemical coupled modeling of a lithium-ion cell', *Proc. ECS*.

Hui, S. (2010) 'Multi-objective optimization for hydraulic hybrid vehicle based on adaptive simulated annealing genetic algorithm', *Engineering Applications of Artificial Intelligence*, vol. 23, no. 1, pp. 27-33.

Johri, R., and Filipi, Z. (2009) 'Low-cost Pathway to Ultra Efficient City Car: Series Hydraulic Hybrid System with Optimized Supervisory Control', SAE Paper 2009-24-0065.

Karden, E., Ploumen, S., Fricke, B., Miller, T., and Snyder, K. (2007) 'Energy storage devices for future hybrid electric vehicles', *J. Power Sources*, vol. 168, pp. 2-11.

Lin, C.-C., Peng, H, Grizzle, J. W., and Kang, J.-M. (2003) 'Power management strategy for a parallel hybrid electric truck', *IEEE Trans. Control Systems Technology*, vol. 11, no. 6, pp. 830-849, 2003.

Lin, C.-C., Peng, H, Grizzle, J. W, (2004) 'A stochastic control strategy for hybrid electric vehicles', Proc. American Control Conference, pp. 4710-4715, Boston, MA, USA.

Patil, R., Adornato, B., and Filipi, Z. (2009) 'Impact of Naturalistic Driving Patterns on PHEV Performance and System Design', SAE Paper 2009-01-2715.

Patil, R., Adornato, B., and Filipi, Z. (2010) 'Design Optimizaion of a Series Plug-in Hybrid Electric Vehicle for Real-World Driving Conditions', SAE Paper 2010-01-0840.

Sciarretta, A., Back, M., and Guzzella. L. (2004) 'Optimal Control of Parallel Hybrid Electric Vehicles', *IEEE Trans. Control Systems Technology*, vol. 12, no. 3 pp. 352-363.

Sharer, P., Rousseau, A., Pagerit, S., and Nelson, P. (2007) 'Midsize and SUV vehicle results for plug-in HEV component requirements', SAE Paper 2007-01-0295.

Smith, K, and Wang, C.-Y. (2005) 'Pulse Discharge Power Availability of a Lithium-Ion Hybrid Vehicle Battery Pack', SAE Paper 2005-01-3464.

Smith, K, and Wang, C.-Y. (2006) 'Power and Thermal Characterization of a lithium-ion battery pack for hybrid-electric vehicles', *J. Power Sources*, vol. 160, pp. 662-673.

Smith, K, and Wang, C.-Y. (2006) 'Solid state diffusion limitations on pulse operation of a lithium ion cell for hybrid electric vehicles', *J. Power Sources*, vol. 161, pp. 628–639.

Surampudi, B., Nedungadi, A., Ostrowski, G., Montemayor, A., and Gruenewald, H. (2009) 'Design and Control Considerations for a Series Heavy Duty Hybrid Hydraulic Vehicle', SAE Paper 2009-01-2717.

West, M. J., Bingham, C. M., and Schofield, N. (2003) 'Predictive control for energy management in all/more electric vehicles with multiple energy storage units', *IEEE International Electric Machines and Drives Conference, 2003. IEMDC'03.*: vol. 1, pp. 222-228.

Wu, B., Lin, C.-C., Filipi, Z., Peng, H., and Assanis, D. (2004) 'Optimal Power Management for a Hydraulic Hybrid Delivery Truck', *J. Vehicle System Dynamics*, vol. 42, no. 1-2, pp. 23-40.